sustainability

MDPI

Article

Thermal and CFD Analyses of Sustainable Heat Storage-Based Passive Greenhouse Dryer Operating in No-Load Condition

Asim Ahmad [1], Om Prakash [2], Shailesh Kumar Sarangi [3], Prashant Singh Chauhan [4], Rajeshwari Chatterjee [5], Shubham Sharma [6,7,*], Raman Kumar [8], Sayed M. Tag [9], Abhinav Kumar [10], Bashir Salah [11] and Syed Sajid Ullah [12,*]

1 Faculty of Engineering and Applied Sciences, Usha Martin University, Ranchi 835103, India
2 Department of Mechanical Engineering, Birla Institute of Technology, Ranchi 835215, India
3 Department of Mechanical Engineering, Srinath University, Jamshedpur 831013, India
4 Department of Mechanical Engineering, Gaya College of Engineering, Gaya 823003, India
5 Department of Chemical Engineering, Birla Institute of Technology, Ranchi 835215, India
6 Mechanical Engineering Department, University Centre for Research and Development, Chandigarh University, Mohali 140413, India
7 School of Mechanical and Automotive Engineering, Qingdao University of Technology, Qingdao 266520, China
8 Department of Mechanical and Production Engineering, Guru Nanak Dev Engineering College, Ludhiana 141006, India
9 Faculty of Engineering, Future University in Egypt, New Cairo 11835, Egypt
10 Department of Nuclear and Renewable Energy, Ural Federal University Named after the First President of Russia, Boris Yeltsin, 19 Mira Street, 620002 Ekaterinburg, Russia
11 Industrial Engineering Department, College of Engineering, King Saud University, P.O. Box 800, Riyadh 11421, Saudi Arabia
12 Department of Information and Communication Technology, University of Agder (UiA), N-4898 Grimstad, Norway
* Correspondence: shubham543sharma@gmail.com or shubhamsharmacsirclri@gmail.com (S.S.); syed.s.ullah@uia.no (S.S.U.)

Abstract: This article presents a comprehensive study on thermal and computational fluid dynamics (CFD) analysis of an innovative greenhouse dryer designed for passive operation under a no-load condition. The dryer incorporates hybrid thermal storage at the floor and a reflective mirror with thermocoal as the north wall, transforming a classical even-span greenhouse dryer into an efficient and effective system. The experimentation was conducted under clear sky conditions, with variations in global solar radiation (GSR) ranging from 166.6 to 1209 W/m^2, resulting in an average value of 875.9 W/m^2. The variations in GSR influenced other ambient parameters, including ambient temperature (28.7 °C to 35.6 °C), ambient relative humidity (33.2% to 45.7%), and ambient wind speed (0.1 to 1.02 m/s). Indoor parameters of the proposed dryer, such as inside temperature (31 °C to 47.35 °C), inside relative humidity (31.1% to 39.1%), ground temperature (44.2 °C to 70.6 °C), and outlet temperature (29 °C to 45.35 °C), were measured hourly. The average values of these parameters were 41.25 °C, 35.31%, 61.65 °C, and 39.25 °C, respectively. Quantitative parameters, including heat loss, overall heat transfer coefficient, coefficient of diffusion, and instantaneous efficiency, were calculated to evaluate the dryer's performance. The proposed dryer exhibited an improved range of overall heat transfer coefficients (3.87 to 5.03 W/m^2 K) compared to the modified greenhouse dryer under passive mode and the conventional greenhouse under passive mode. CFD analysis provided temperature distribution plots showing a progressively increasing range of temperatures near the trays, ranging from 310 K to 335 K, suitable for natural convection drying. The findings highlight the superior performance of the innovative dryer compared to contemporary systems. This research contributes to the advancement of drying technology and holds potential for applications in the agriculture and food processing industries.

check for updates

Citation: Ahmad, A.; Prakash, O.; Sarangi, S.K.; Singh Chauhan, P.; Chatterjee, R.; Sharma, S.; Kumar, R.; Tag, S.M.; Kumar, A.; Salah, B.; et al. Thermal and CFD Analyses of Sustainable Heat Storage-Based Passive Greenhouse Dryer Operating in No-Load Condition. *Sustainability* **2023**, *15*, 12067. https://doi.org/10.3390/su151512067

Academic Editors: Irfan Anjum Badruddin Magami, Sarfaraz Kamangar, C. Ahmed Saleel and T. M. Yunus Khan

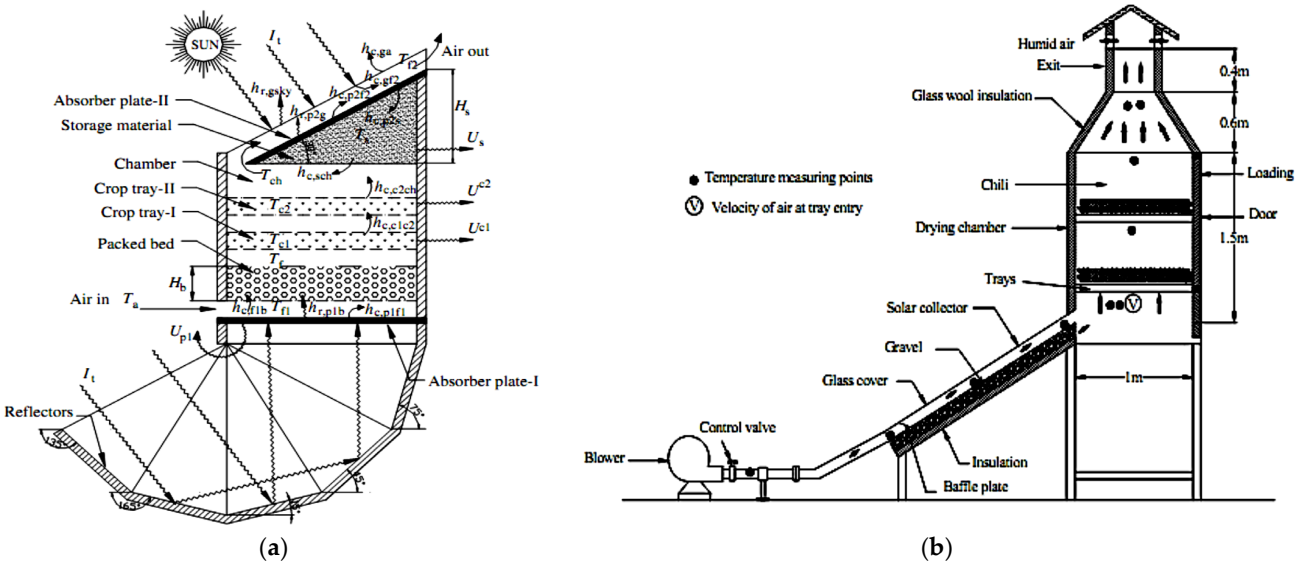
Received: 6 March 2023
Revised: 3 July 2023
Accepted: 18 July 2023
Published: 7 August 2023

Copyright: © 2023 by the authors. Licensee MDPI, Basel, Switzerland. This article is an open access article distributed under the terms and conditions of the Creative Commons Attribution (CC BY) license (https://creativecommons.org/licenses/by/4.0/).

Keywords: greenhouse dryer; thermal analysis; computational fluid dynamics; no-load condition; natural convection

1. Introduction

Drying is a process to reduce moisture from a product, which is one of the ancient techniques used for food or agricultural products for safe storage [1,2]. Food products, particularly fruits and vegetables require hot climatic conditions in the temperature range of 45 to 65 °C for safe drying to keep their edible and nutritional stuffs unchanged [3,4]. Food preservation is the need to reduce food losses and cost-effective transportation, which results from economic final products [2,3]. It has been widely accepted as an important tool for a long time [5]. Therefore, well-designed energy-efficient drying technologies are required [6,7]. Developing countries are facing an energy crisis; hence, solar drying is the most attractive drying technology since sun-radiant energy is available in abundant amounts [8]. However, solar radiation is limited to use during sunshine hours due to its intermittent nature and non-availability at night [9]. Hence, heat storage is required to store or absorb solar energy during sunshine hours and that can be utilized after sunshine hours [10]. The hybrid single tank thermocline designed by incorporating a heat concrete block in between D mannitol and adipic acid is an efficient thermal storage system [11]. It can be three types (a) sensible heat storage, (b) latent heat storage, and (c) thermochemical (combination of sensible and latent heat storage) storage [12]. In sensible heat storage, the temperature increases of any liquid or solid without any phase changes but in latent heat storage phase change occurs in heat-storing material [13]. While in a thermochemical heat storage system the heat energy is stored in the form of chemical bonds, and it releases this stored energy by reversible chemical reaction [14]. Solar drying systems can be classified as direct drying and indirect drying systems. A direct drying system is where crops are directly exposed to sun radiation inside the dryer, whereas in an indirect system, an air heating system is required and crops are kept in another cabinet (Figure 1a,b) [15].



(**a**) (**b**)

Figure 1. (**a**) direct drying system and (**b**) indirect drying system (Adapted from the reference [5]).

Generally, greenhouse dryers and tunnel dryers come under the category of direct drying systems. Various researchers have applied heat storage material in greenhouse drying systems. A greenhouse dryer was developed and integrated with PCM ($CaCl_2 \cdot 6H_2O$) on the north wall [16]. The rise of inside air temperature was found to be in the range of 6 to 12 °C and the cover temperature was 4 to 5 °C due to the use of 4 cm thick PCM on the

north wall as a thermal storage. A natural convection solar tunnel drier was developed using a rock bed to examine its performance for copra drying [17].

Rock beds were used as sensible thermal storage. Simultaneously, experiments were performed without a rock bed to compare its result. The utilization of heat storage material improved the drying efficiency of the dryer with rock bed by 2–3%. A natural convection greenhouse dryer was developed using different types of heat storage materials like concrete, rock-bed, and sand to evaluate their performance [18]. The drying system reduced the moisture content of coconuts from 52% to 7% wet basis using concrete heat storage material for a total of 78 h and successively reduced drying time by 55% as compared to open sun drying. For the same heat storage material, sand took 66 h and reduced 62% drying time; however, for heat storage material, the rock-bed acquired only 53 h and reduced drying time by 69%. The drying efficiency of the dryer with thermal storage material was found to always be higher at 11.6%, 11%, and 9.5% using rock-bed, sand, and concrete, respectively. A north-wall insulated greenhouse dryer was developed with a heating collector for gooseberry and bitter gourd drying for complete dehydration of moisture [15]. The study yielded significant results by effectively reducing the drying time. In this research, a greenhouse dryer was developed and integrated with various types of heat storage beds, including gravel beds, black-painted gravel beds, ground beds, and concrete floor beds [19]. One of the notable findings was that the black-painted gravel bed achieved a maximum room air temperature of 64.4 °C, which corresponds to a heat gain percentage of 53%. This demonstrates the effectiveness of the integration in terms of heat transfer and performance improvement.

Another aspect of the study focused on investigating the impact of different corrugation interruptions on thermohydrodynamic characteristics and heat transfer performance using 3D corrugated tubes. The researchers explored the flow field and heat transfer enhancement by combining corrugated tubes with twisted tape within a 3D circular tube, considering variations in dimple configurations. The objective was to develop correlations for improved thermo-hydraulic flow and heat transfer performance. Furthermore, the researchers conducted an analysis to examine the flow structure and heat transfer improvement in a 3D circular tube utilizing various axial groove turbulator configurations. They carried out a numerical study to investigate the effect of turbulators on thermal flow and heat performance in a 3D pipe [20].

Despite the existing studies on greenhouse dryers and heat storage materials, there is a research gap in understanding the specific effects of different heat storage materials on the drying efficiency of greenhouse dryers. While previous research has explored the use of concrete, rock-bed, and sand as heat storage materials, there is a need for further investigation to compare their performance and determine the optimal heat storage material for improved drying efficiency. Additionally, there is a lack of studies focusing on the integration of reflective mirrors, insulation, and thermal storage to minimize heat loss and maximize solar radiation utilization in greenhouse dryers. This research gap highlights the need for a comprehensive study that combines these elements to enhance the energy efficiency and overall performance of greenhouse dryers.

The present experimental work focuses on the design and modernization of a greenhouse dryer with the objective of reducing energy consumption under passive mode. The novelty of this study lies in the application of a reflective mirror on the north side and the use of a 10 mm thick polystyrene sheet as insulation to maximize solar radiation utilization and minimize heat loss from the north wall. Additionally, thermal storage material is incorporated to mitigate conductive heat loss from the ground. These modifications aim to enhance the effectiveness and performance of the dryer.

The determination of the overall heat transfer coefficient, calculation of heat loss, evaluation of the instantaneous efficiency factor, and the use of computational fluid dynamics (CFD) analysis are key objectives of this research. These parameters provide essential insights into the performance and effectiveness of the dryer, which are crucial for optimizing its operation and energy efficiency.

The applications of this research extend to the field of sustainable agriculture, specifically in the area of crop drying. Efficient and effective greenhouse dryers can contribute to preserving the quality and nutritional value of agricultural produce [21,22]. The findings of this study can benefit the agricultural community, farmers, researchers, and policymakers working towards sustainable food production and post-harvest management [23–25]. The knowledge gained from this research can help optimize drying processes, reduce energy consumption, and improve the overall quality of dried crops, leading to economic and environmental benefits.

2. Material and Method

2.1. Experimental Setup

The proposed system is the modified version of the classical even-span greenhouse dryer. There are two major modifications incorporated in the classical system, namely in the north wall and ground of the dryer. In the north wall of the greenhouse dryer where maximum heat loss happens in the classical dryer, the transparent wall is replaced by a reflecting mirror with thermocoal. A detailed description of the system is presented in Table 1. A schematic diagram and a real view of the proposed system are presented in Figure 2a,b. Reflecting mirrors are used to restrict outgoing radiation and heat. Thermocoal is kept outside of the glass should no heat loss happen through the glass. By this arrangement, a substantial amount of heat can be preserved. This enhances the drying efficiency of the proposed system [26–28].

Table 1. Description of the proposed system.

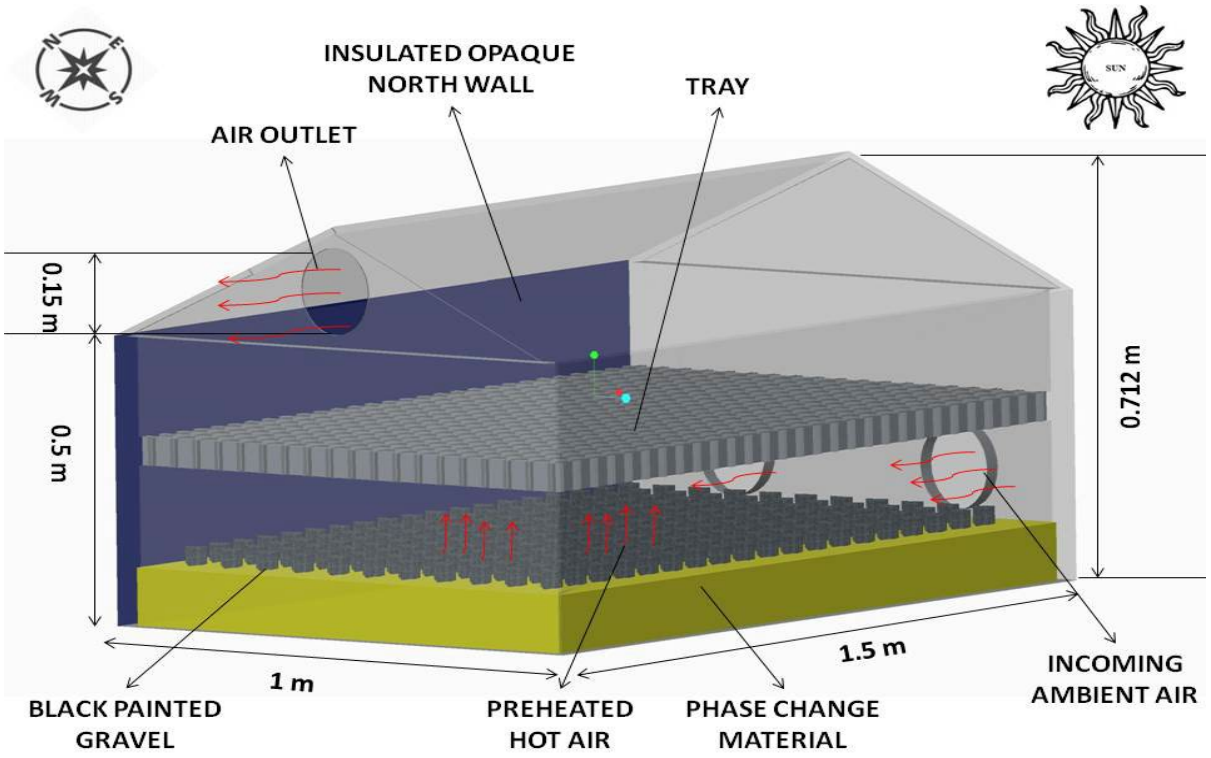
Sl. No.	Parameters	Values
1	Length	1.5 m
2	Width	1 m
3	Height	0.712 m
4	Gravel	29 kg
5	PCM	35 kg
6	Load capacity	4.0 kg
7	Load surface area	1 m^2
8.	Mirror area	0.75 m^2
9.	Thermocoal	0.75 m^2

The ground floor of the dryer is modified. Heat storage material is applied on the floor of the dryer so that system thermal performance can be enhanced. Dual-layer thermal storage material is used where the bottom layer is the phase change material (latent heat storage material) and the upper layer is gravel (sensible heat storage material).

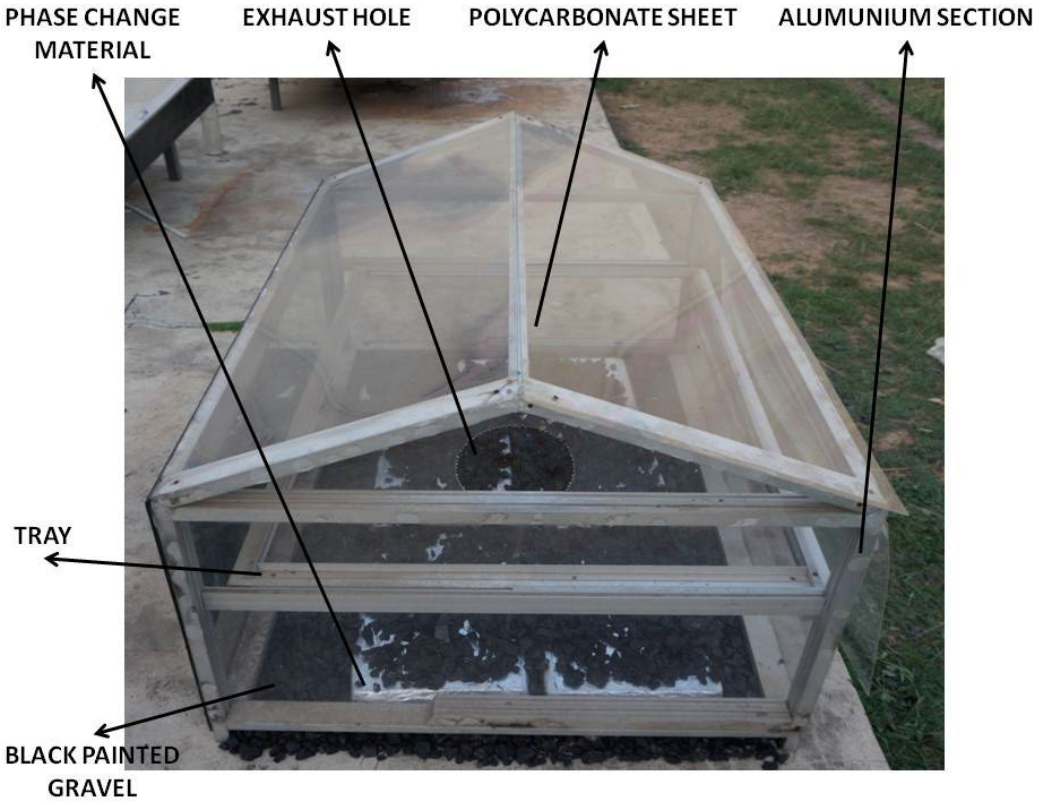
Firstly, paraffin wax is mixed with black painted gravel and put above the black PVC sheet. This makes a 50 mm thicker layer of this storage material at the bottom of the greenhouse dryer. Thermo-physical properties of paraffin wax are presented in Table 2.

Table 2. Thermo-physical properties of paraffin wax (RT35).

Melting Temperature of Paraffin Wax	35 °C
Kinematic viscosity (m^2/s)	3.3×10^{-6}
Density (kg/m^3)	880/760 (liquid/solid)
Thermal Conductivity	25 W/m·K
Specific heat capacity (kj/kg.K)	1.8/2.4 (liquid/solid)
Latent heat (kj/kg)	157



(**a**)



(**b**)

Figure 2. (**a**) Schematic View of Heat Storage based Passive Greenhouse dryer [5]. (**b**) Real View of Heat Storage based Passive Greenhouse dryer.

2.2. Instrumentation

The proposed system is examined critically on an hourly basis with the help of technically effective instruments. Details of the instruments are presented in Table 3. Both indoor and outdoor/ambient parameters are observed to clearly understand the thermal behavior of the proposed system. The following ambient parameters are observed: global solar radiation, ambient temperature, ambient relative humidity, and wind speed. However, the following parameters are observed at the outlet point: outlet temperature, outlet relative humidity, and air speed. The following parameters are observed inside the dryer namely ground temperature, inside temperature, and inside relative humidity.

Table 3. Details of instrument used.

Sl. No.	Device	Company	Model No.	Range	Least Count	Purpose of Measurement
1	Solar Power meter	Temmars	TM-207	0–1999 W/m^2	1	Solar radiation
2	Infrared thermometer	Hetect	H-1020	−50–550 °C	1	Non-contact temperature
3	Hot wire anemometer	HTC	AVM-08	0.1–25 m/s	0.1	Wind speed
4	Hygrometer	Dhruv	Pro	0–99%	1	Relative humidity
5	Thermometer	Thremisto	-	−50–300°	0.1	Temperature

2.3. Experimentation

The proposed system is observed on an hourly basis from 9 a.m. to 5 p.m. to identify its thermal behavior. An experiment was conducted on 15 February 2022 at the University campus of Birla Institute of Technology Mesra, Ranchi-India.

3. Performance and CFD Analysis

3.1. Data Reduction

The following mathematical parameters need to be calculated to properly evaluate the thermal performance of the proposed system. Such parameters are the overall heat transfer coefficient, dimensionless numbers, coefficient of diffusion, heat loss, and instantaneous thermal loss efficiency factor. Overall heat transfer coefficient factor further depends upon other factors namely radiative heat transfer coefficient, and convective heat transfer coefficients [29,30]. These parameters are evaluated based on the following Equation (1).

$$\frac{1}{U} = \left(\frac{1}{h}\right) + \left(\frac{l}{K}\right) + \left(\frac{1}{h_{can}}\right) \tag{1}$$

Connellan [8] proposed a different relation for 'U' as in Equation (2):

$$U = 3.96 + 1.02V_{wd} \tag{2}$$

It can be analyzed by using Equations (3)–(6):

$$h = h_g + h_r + h_{evp} \tag{3}$$

$$h_{can} = 7.2 + 3.8V_{wd} \tag{4}$$

$$h_r = \frac{\sigma\varepsilon\left[\left(T_{grd} + 273.15\right)^4 - \left(T_{rm} + 273.15\right)^4\right]}{\left(T_{grd} - T_{rm}\right)} \tag{5}$$

$$h_{grd} = 0.884\left(T_{grd} - T_{rm} + \frac{\left[P\left(T_{grd}\right) - \gamma P(T_{rm})\right]\left(T_{grd} - 273\right)}{268.9 \times 10^3 - P\left(T_{grd}\right)}\right)^{\frac{1}{3}} \quad (6)$$

Here, h_{evp} can be neglected as it is very small.

The dimensionless number can be evaluated by using Equations (7)–(10).

$$Gr = \frac{{W_1}^3 g\beta_1 \Delta T}{v^2} \quad (7)$$

$$Ra = Gr.Pr = \frac{{W_1}^3 g\rho^2 C_p \Delta T^3}{K\mu_1} \quad (8)$$

$$Nu = \frac{hW_1}{K} \quad (9)$$

$$Pr = \frac{C_p \mu_1}{K} \quad (10)$$

The parameter W can be evaluated by using Equation (11) as the floor of the dryer is in rectangular shape:

$$W = \frac{L_1 + B_1}{2} \quad (11)$$

Instantaneous heat loss can be evaluated by Equation (12):

$$\eta_1 = \frac{U\sum A_{in}(T_{rm} - T_{amb})}{IA_{grd}} \quad (12)$$

Coefficient of diffusion can be evaluated by Equation (13):

$$C_{dif} = \frac{(1 - \eta_1)IA_{grd}}{nA_{vn}\sqrt{\frac{2\Delta P_1}{\rho_1^+ r}\Delta P_1}} \quad (13)$$

Heat loss can be calculated by Equation (14):

$$Q_{ls} = C_{dif}A_{vn}\sqrt{\frac{2\Delta P_1}{\rho_1^+ r}\Delta P_1} \quad (14)$$

3.2. Mathematical Expressions for CFD Modelling

The governing equations considered in the present CFD analysis are based on the following Navier–Stokes equations [20,31,32]:

Continuity equation

$$\frac{\partial \rho}{\partial t} + \nabla.(\rho V) = S_m \quad (15)$$

Momentum Equation

$$\frac{\partial(\rho V)}{\partial t} + \nabla.(\rho vv) = -\nabla p + \rho g + \nabla(T) + F \quad (16)$$

Energy equation

$$\frac{\partial(\rho E)}{\partial t} + \nabla.[V(\rho E + p)] = \nabla.\left[k_{eff}\nabla T - \sum h_j j_j + \left(T_{eff}.V\right)\right] + S_h \quad (17)$$

where v is the fluid flow velocity, ρ is the density, F is the applied external force, S_m is the added mass source, ρg is the gravitational force, S_h represents the sensible enthalpy source, E represents the total energy contained by the fluid, and p is the pressure.

The Standard k-ε Model

The transport equations for turbulence kinetic energy (k) and rate of dissipation (ε) are given as:

$$\frac{\partial(\rho k)}{\partial t} + \frac{\partial(\rho k u_i)}{\partial x_i} = \frac{\partial(\rho k u_i)}{\partial x_j}\left[\left(\mu + \frac{\mu}{\sigma_k}\right)\frac{\partial k}{\partial x_j}\right] + G_k + G_b + \rho\varepsilon - Y_M + S_k \quad (18)$$

$$\frac{\partial(\rho \varepsilon)}{\partial t} + \frac{\partial(\rho \varepsilon u_i)}{\partial x_i} = \frac{\partial}{\partial x_j}\left[\left(\mu + \frac{\mu_t}{\sigma_\varepsilon}\right)\frac{\partial \varepsilon}{\partial x_j}\right] + C_{1\varepsilon}\frac{\varepsilon}{k}(G_k + C_{3\varepsilon}G_b) - C_{2\varepsilon}\frac{\varepsilon^2}{k} + S_\varepsilon \quad (19)$$

G_k and G_b denote the development of turbulence kinetic energy due to the mean velocity gradients and buoyancy, respectively. The contribution of the fluctuating dilatation is represented by Y_M. The turbulence Prandtl numbers for k and ε are represented, respectively, by σ_k and σ_ε. S_k and S_ε denote the source terms for k and ε, respectively, and the constants are represented by $C_{1\varepsilon}$, $C_{2\varepsilon}$, and $C_{3\varepsilon}$.

$C_{1\varepsilon} = 1.44$, $C_{2\varepsilon} = 1.92$, $\sigma_k = 1.0$, $\sigma_\varepsilon = 1.3$.

The following combination of k and ε yields the eddy viscosity,

$$\mu_t = \rho C_\mu k^2/\varepsilon \quad (20)$$

where $C_\mu = 0.09$, is the model constant.

The term G_k is modeled identically for all the k and ε models (Standard, RNG, and Realizable).

$$G_k = \mu_t S^2 \quad (21)$$

where S stands for the modulus of the mean rate-of-strain tensor and is given as,

$$S = \sqrt{2 S_{ij} S_{ij}} \quad (22)$$

The turbulence developed by buoyancy is given by

$$G_b = \beta g_i \mu_t / pr\, \partial T/\partial_{xi} \quad (23)$$

where Pr_t stands for the turbulent-Prandtl number, g_i stands for the ith direction gravitational vector component. Pr_t is 0.85 for the standard and realizable k-ε models, whereas it is $1/\alpha$ for the RNG k-ε model.

$$\left|\frac{(\alpha - 1.3929)}{(\alpha_0 - 1.3929)}\right|^{0.6321}\left|\frac{(\alpha - 2.3929)}{(\alpha_0 - 2.3929)}\right|^{0.3679} = \frac{\mu_{mol}}{\mu_{eff}}$$

where $\alpha_0 = 1.0$.

The contribution of the fluctuating dilatation in compressible turbulence to the overall dissipation rate (Y_M)

$$Y_M = 2\rho\varepsilon M_t^2 \quad (24)$$

The turbulent Mach Number M_t is defined as

$$M_t = \sqrt{k/\alpha^2} \quad (25)$$

where α is the speed of the sound ($a = \sqrt{\gamma RT}$).

The radiative transfer equation (RTE) for an absorbing, emitting, and scattering medium at position $\vec{r}$ in the direction $\vec{s}$ is,

$$\left(\frac{dI\left(\vec{r},\vec{s}\right)}{ds}\right)+(\alpha+\sigma_s)I\left(\vec{r},\vec{s}\right)=\frac{an^2\sigma T^4}{\pi}+\frac{\sigma_s}{4\pi}\int I\left(\vec{r},\vec{s}\right)\varphi\left(\vec{r},\vec{s}\right)d\Omega \quad (26)$$

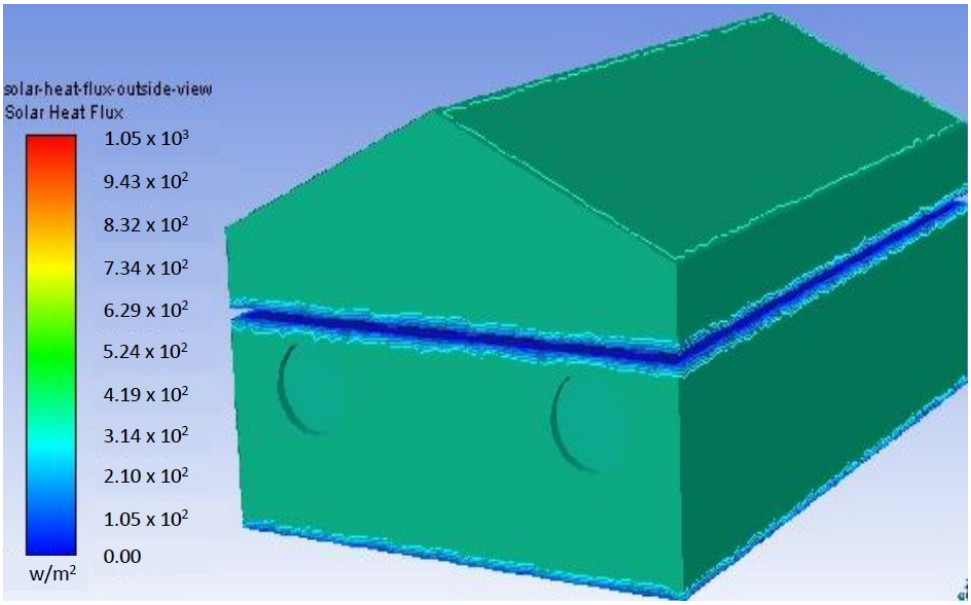
where $\vec{r}$ is the position vector, $\vec{s}$ stands for the direction vector, $\vec{s\prime}$ represents the vector along scattering direction, s denotes the path length, a is the absorption coefficient, n is the refractive index, σ_s stands for the scattering coefficient, σ is the Stefan–Boltzmann constant (5.669×10^{-8} W/m^2 K^4), I represents the radiation intensity, which relies on $\vec{r}$ and $\vec{s}$, T stands for the local temperature, φ denotes the phase function, and Ω denotes the solid angle.

3.3. Boundary Conditions

The boundary conditions considered have been evaluated from the average of the experimental measurements of the present study. In Ansys 19.2, a solar ray tracing model was employed to evaluate solar heat flux. Figure 3a,b shows the inside and outside heat flux variation. Table 4 shows the boundary conditions on different surfaces of the greenhouse dryer.

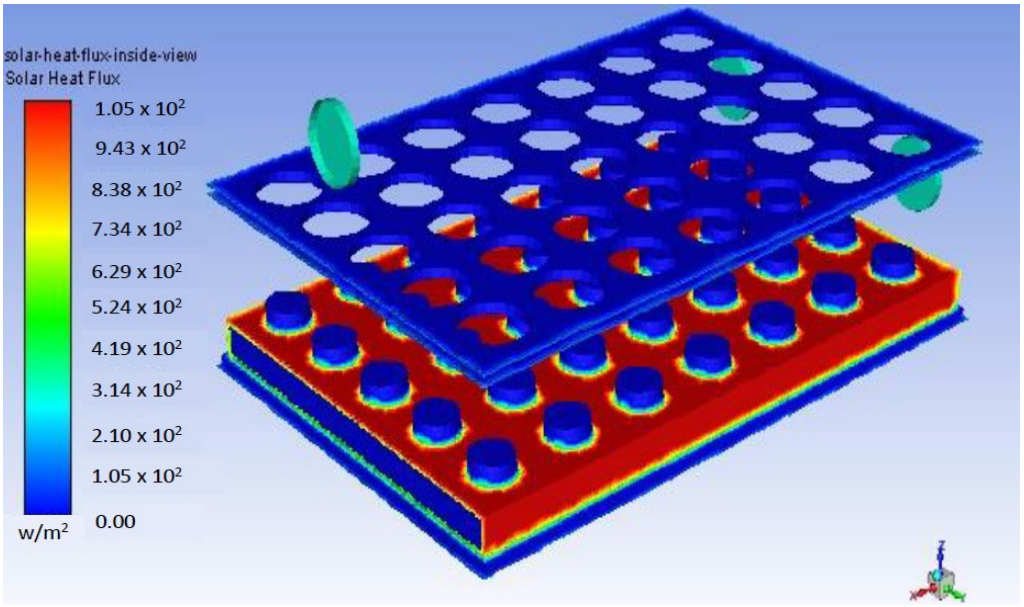
Table 4. Boundary Conditions for the Greenhouse Dryer.

Surface	Temperature Value
East Wall	309.96 K
West Wall	307.25 K
South Wall	310.36 K
North Wall	306.23 K



(**a**)

Figure 3. *Cont.*



(**b**)

Figure 3. Distribution of Solar heat flux: (**a**) Outside view; (**b**) inside view.

3.4. Numerical Method

The geometric model for the studied configurations has been developed using the 3D geometry creator "Design Modular" of the Ansys Workbench (V19.2). The working fluid is considered air, which has a density and viscosity of 1.225 kg/m^3 and 1.885 $\times$ 10^{-5} kg/ms, respectively. At all solid surfaces, the no-slip boundary condition is prescribed. The simulations are carried out using the Standard K-ε turbulence model, which is also utilized to model the entire computational domain and estimate the values of performance parameters. The SIMPLEC (semi-implicit method for pressure-linked equation consistent) algorithm is used to assure the pressure and velocity coupling. The discretization of pressure was achieved with a standard scheme and for momentum discretization, the QUICK scheme was considered. The second-order upwind scheme discretizes the energy equations and the dissipation rate. For all the conservation equations, the solver's tolerance is set to 10^{-5}. Although the convergence of residuals is reached at about 1000 iterations, the simulations are run for additional 300 iterations to ensure higher accuracy.

3.5. Grid Independency

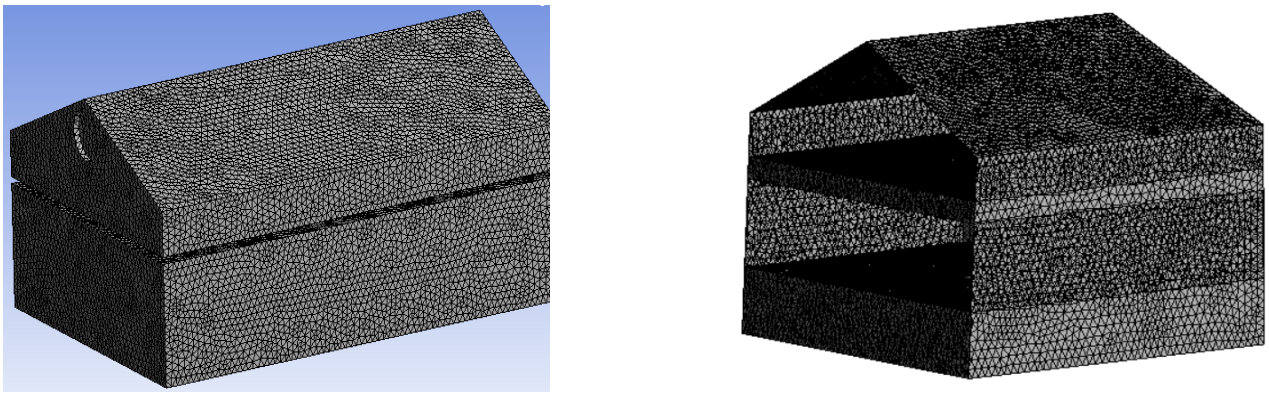
The computational domain for each of the considered models has been meshed using the tetrahedral meshing elements. Three levels of meshes have been considered to ensure grid independence of the solutions, viz: 262,856, 522,887, and 758,982 meshing elements. However, the solutions in terms of outlet air velocity remain unchanged when the mesh size is increased from 522,887 to 758,982 (Table 5). This suggests the attainment of grid independence of the results. Thus, for the grid generation of the numerical models, the element size corresponding to 522,887 is considered for the present analysis. The generated grid for the entire computational domain and the cut section model has been shown in Figure 4. Table 6 has exhibited the variation in maximum air outlet velocity with mesh size.

Table 5. The Convergence Criteria for the Residuals.

Residuals	Criteria
Continuity	10^{-5}
x-Velocity	10^{-5}

Table 5. *Cont.*

Residuals	Criteria
y-Velocity	10^{-5}
z-Velocity	10^{-5}
Energy	10^{-5}
k	10^{-5}
Epsilon	10^{-5}



(**a**) (**b**)

Figure 4. Generated mesh for the: (**a**) computational domain; (**b**) Cut-section view of the meshes.

Table 6. Variation in maximum air outlet velocity with mesh size.

Mesh Size	Maximum Air Outlet Velocity
262,856	0.814
522,887	0.837
758,982	0.837

Table 7 shows the comparison of the experimental model and the numerical model. The temperature at the outlet of the dryer is measured with a digital thermometer for different hours on 21 June 2021. This experimental result for the outlet air temperature is then compared with the CFD results. The maximum average deviation is below 5%, which confirms the reliability of the considered computational model for the performance estimation of the greenhouse dryer.

Table 7. Comparison of experimental and CFD results for outlet temperature on hourly basis for the selected day (21 June 2021) at location Ranchi.

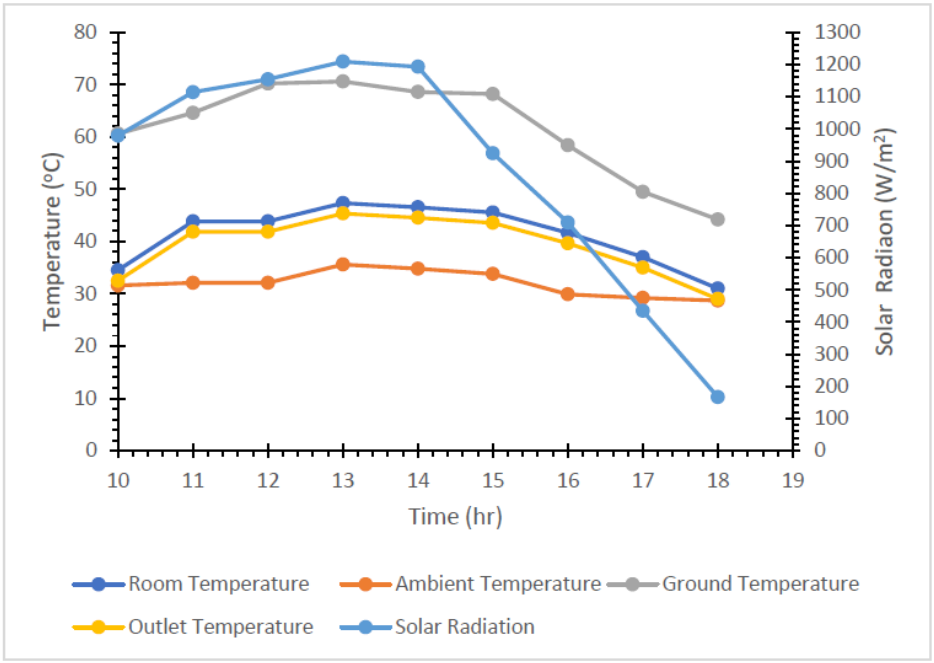
Time (hr)	Outlet Temperature (Experiment) °C	Outlet Temperature (CFD) °C	% Deviation between CFD and Experiment
14	44.55	46.28	3.88
15	43.55	44.08	1.22
16	39.65	40.24	1.48
17	35.00	36.88	5.37
18	29.00	29.45	1.55
	Maximum average deviation		2.7

4. Result and Discussion

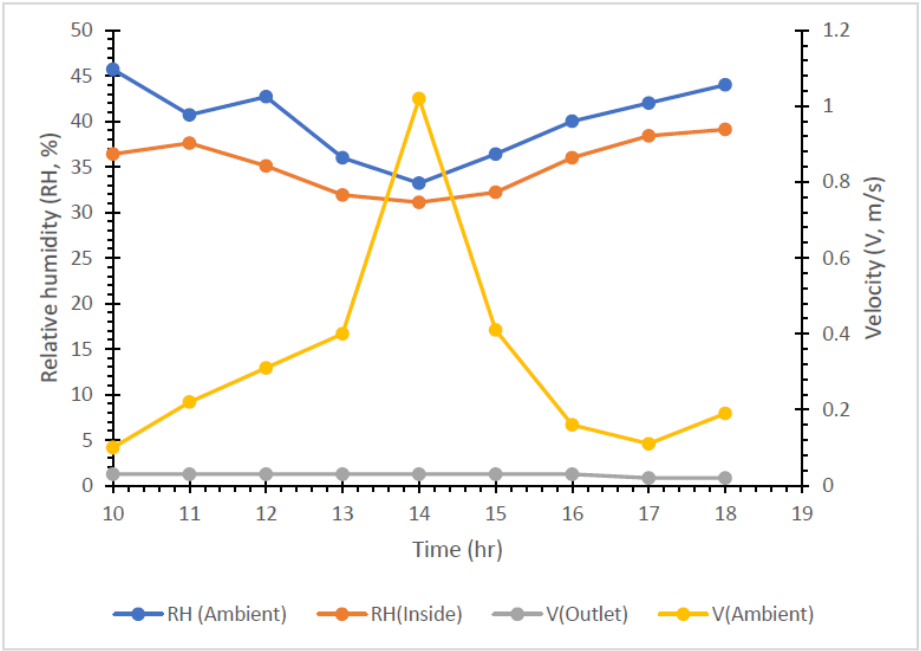
4.1. Variation of Ambient Parameters during Experimentation

The experiment was conducted in a clear sky condition without any abrupt weather change. Global solar radiation (GSR) varies from 166.6 to 1209 W/m^2 with an average value

of 875.9 W/m^2 (as shown in Figure 5a). GSR is the core parameter from which all other parameters depend, which may be ambient temperature, ambient relative humidity, or ambient wind speed. Since the variation of GSR is in a regular pattern so variation of other dependent parameters is also in a regular pattern. Variations of ambient temperature, ambient relative humidity, and ambient wind speed are 28.7–35.6°, 33.2–45.7%, 0.1–1.02 m/s, and average values of these parameters are 31.98 °C, 40.08%, 0.32 m/s, respectively (as shown in Figure 5b).



(**a**)



(**b**)

Figure 5. Variation of the observed parameters during experimentation, (**a**) Variation of temperature (°C) against time (hr), and (**b**) Variation of relative humidity (RH) (%) against time (hr).

4.2. Variation of Indoor Parameters of Proposed Dryer during Experimentation

Inside temperature, inside relative humidity, ground temperature, and outlet temperature are measured on an hourly basis. The variation of these parameters is 31–47.35 °C, 31.1–39.1%, 44.2–70.6 °C, and 29–45.35 °C, respectively. The average value of these parameters is 41.25 °C, 35.31%, 61.65 °C, and 39.25 °C, respectively. Variations of these parameters are regular because these parameters are dependent upon GSR. Due to the storage concept and reflective mirror, inside parameters are quite high which is highly favorable for drying and other thermal applications.

4.3. Variation of Mathematical Parameters

The proposed system properly examined their thermal performance with the help of standard parameters like convective heat transfer coefficient from the ground ($h_{c,gr}$), convective heat transfer coefficient from the canopy ($h_{c,ca}$), radiative heat transfer coefficient from the ground ($h_{r,gr}$), overall heat transfer coefficient (U), heat loss, coefficient of diffusion, dimensionless number and instantaneous thermal loss efficiency factor. Overall heat transfer coefficient depends upon convective and radiative heat transfer coefficients. Hourly variations of these parameters are shown in Figure 6. The variation of $h_{c,gr}$, $h_{c,ca}$, $h_{r,gr}$, and U are 2.47–3.55 W/m^2 K, 7.58–11.08 W/m^2 K, 6.05–7.39 W/m^2 K, and 3.87–5.03 W/m^2 K, respectively, also the average value of these parameters are 3.14 W/m^2 K, 8.43 W/m^2 K, 6.91 W/m^2 K, and 4.28 W/m^2 K, respectively.

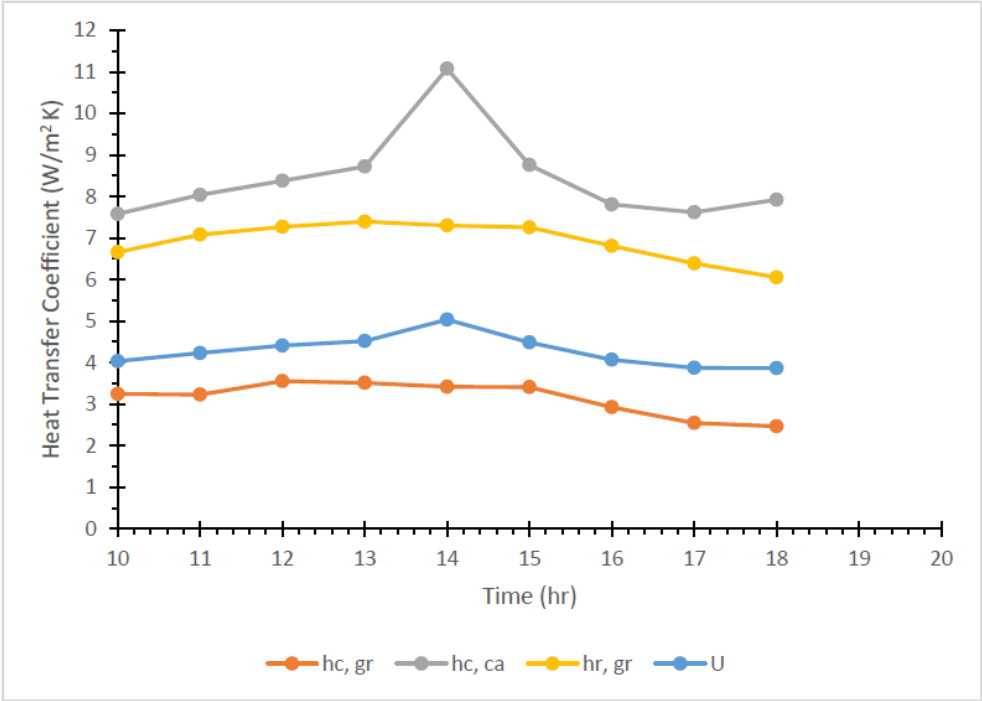


Figure 6. Variation of various heat transfer coefficients.

As per Prakash and Kumar, the characteristic graph for an efficient greenhouse dryer should intercept at zero [33]. A characteristic graph is drawn between instantaneous thermal loss efficiency factor verses ($T_r - T_a/I_r$). A characteristic graph for the proposed system is presented in Figure 7 and intercepts at zero, which validated the modification in the greenhouse dryer.

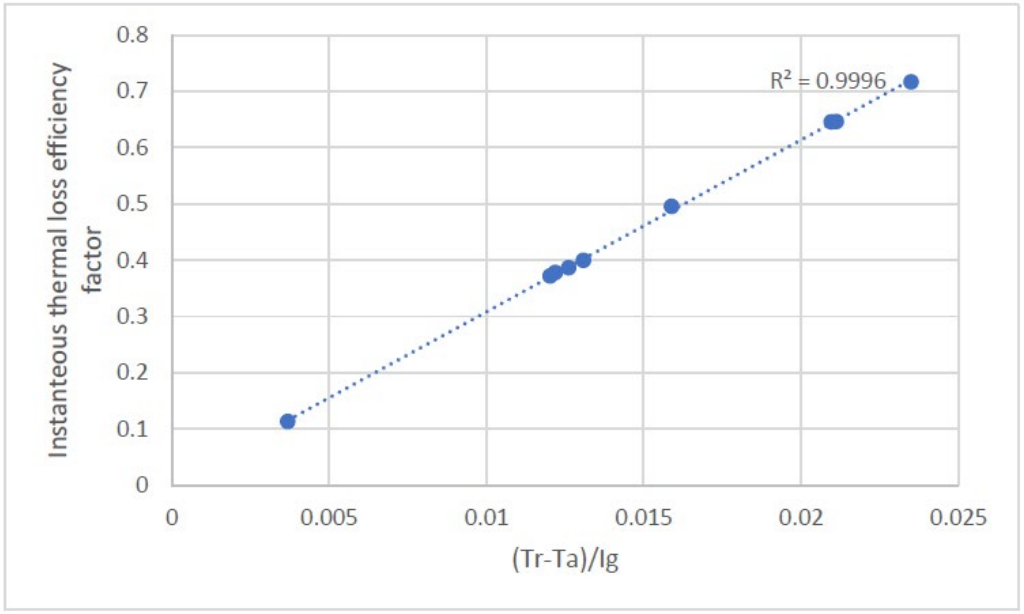


Figure 7. Characteristic graph for the proposed system.

The heat loss and coefficient of diffusivity are calculated for the proposed system based on observed experimental data. Hourly variations of these parameters are shown in Figure 8. Heat loss varies from 105.58 to 549.42 W and the average value is 428.33 W. However, the variation of the coefficient of diffusivity is 0.1531×10^{-3} to 0.1547×10^{-3} and the average value is 0.1541×10^{-3}.

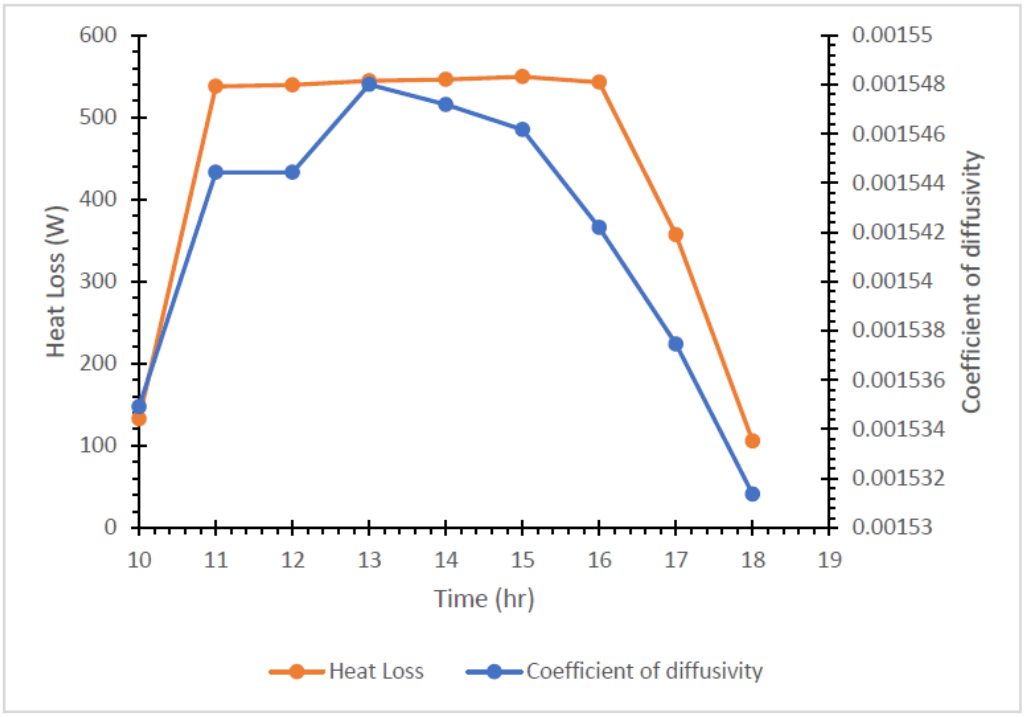
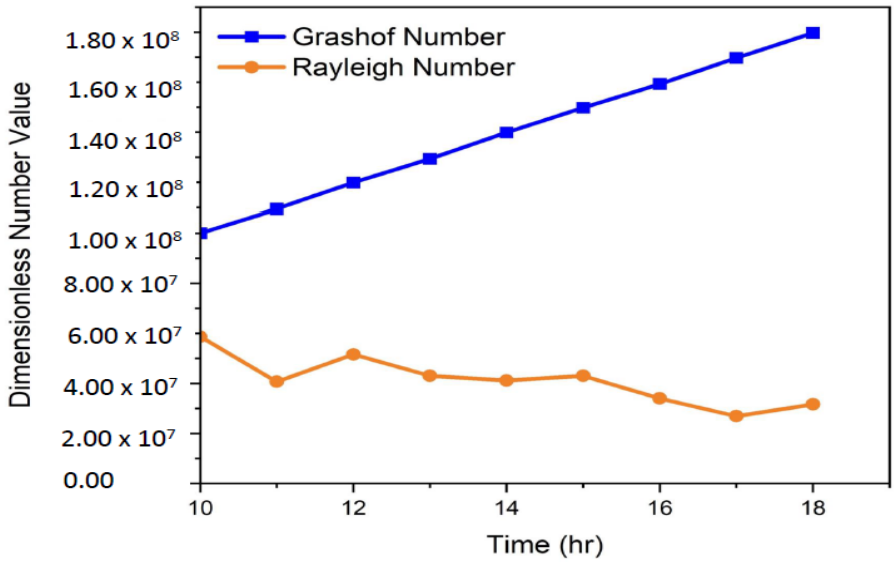


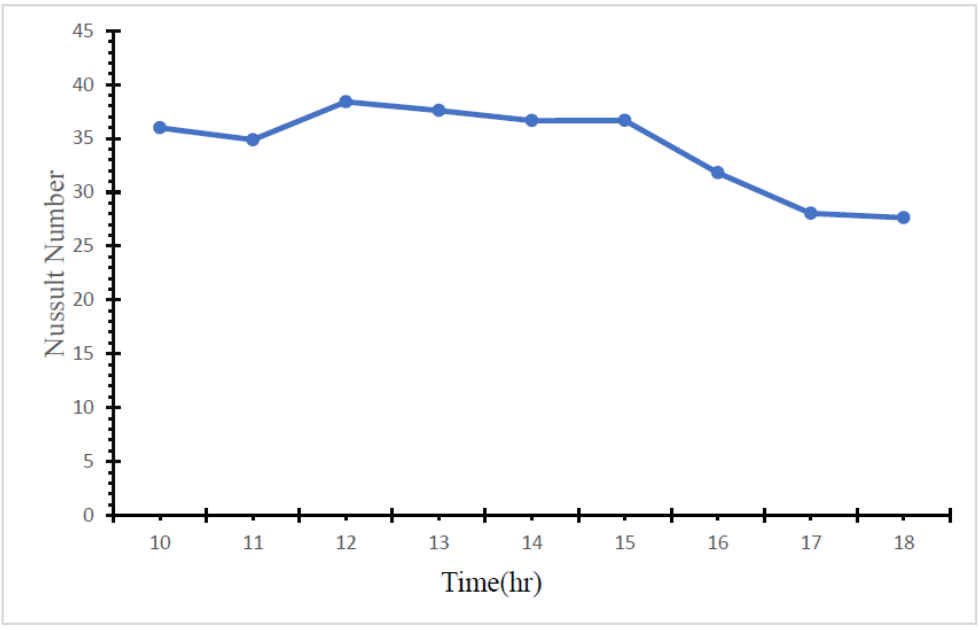
Figure 8. Variation of Heat loss and coefficient of diffusivity.

Various relevant dimensionless numbers are calculated based on the fluid flow of the proposed system. Such numbers are the Grashof number, Prandtl number, Rayleigh number, and Nusselt number. The variation of the Prandtl number during experimentation is found to be almost constant (0.69). The variation of the Grashof number, Rayleigh

number, and Nusselt number are presented in Figure 9a,b. These numbers vary from 10×10^7 to 18×10^7, 2.69×10^7 to 5.85×10^7, and 27.63 to 38.39, respectively. The average value of these parameters is 14×10^7, 4.1110×10^7 and 34.18, respectively.



(**a**)



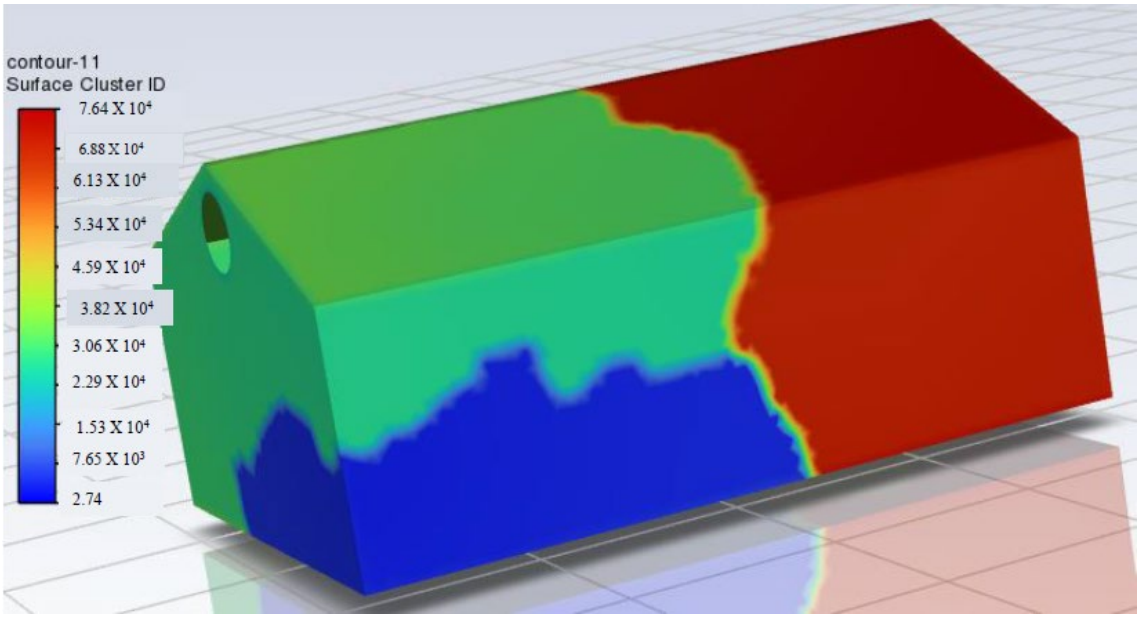
(**b**)

Figure 9. (**a**,**b**) Variation of dimensionless number during experimentation.

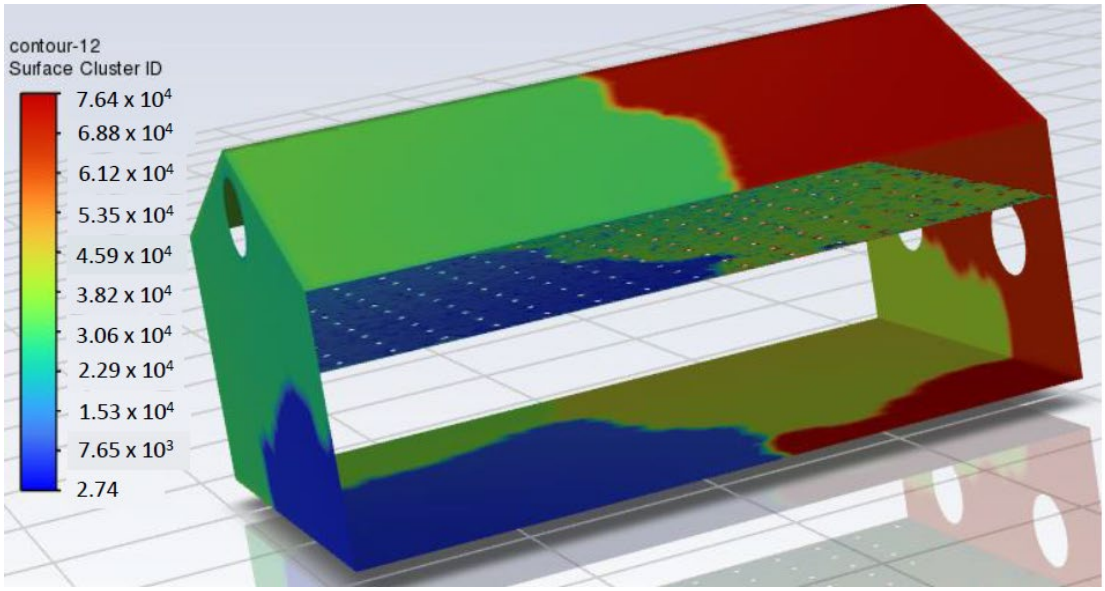
4.4. Temperature Distribution in the Passive Green House Dryer Model

The heat flux distribution obtained from the ray tracing model corresponding to Ranchi city (GMT. +5.30, latitude-23.34, and longitude-85.30) is shown in Figure 10a,b. The day selected was 21 June 2021, which has a maximum radiation value of 1050 W/m^2. The temperature distribution for the GHD for the selected day (21 June 2021) is shown in Figure 10a,b. For the simulations in Ansys Fluent, the direct and diffuse irradiation data obtained from the solar ray tracing is coupled with the discrete ordinate model and the energy model. From the inside view of the greenhouse dryer, it is seen that the maximum temperature is at the base of the GHD, i.e., of the phase change material. The temperature

near the trays varies in the range of 335 K to 310 K, which is appropriate for product drying with natural convection. The maximum velocity at the outlet is 0.837 m/s whereas the inlet velocity is 0.32 m/s.



(**a**)



(**b**)

Figure 10. (**a**) Distribution of Temperature Outside of the GHD. (**b**) Distribution of Temperature inside of the GHD.

4.5. Relative Humidity inside the Solar GHD

The chemical and physical features of the products to be dried are directly influenced by relative humidity. The relative humidity is high where the temperature is low and vice-versa. The spatial distribution of relative humidity is shown in Figure 11. The maximum relative humidity in GHD is 59.8% whereas the minimum relative humidity is 9.9%. It is observed that the higher relative humidity regions overlap with the regions of wet air entering from the outside. Thus, the focus should be made on managing the ventilation

areas during higher humidity periods. Good ventilation management ensures higher efficiency of the greenhouse dryer.

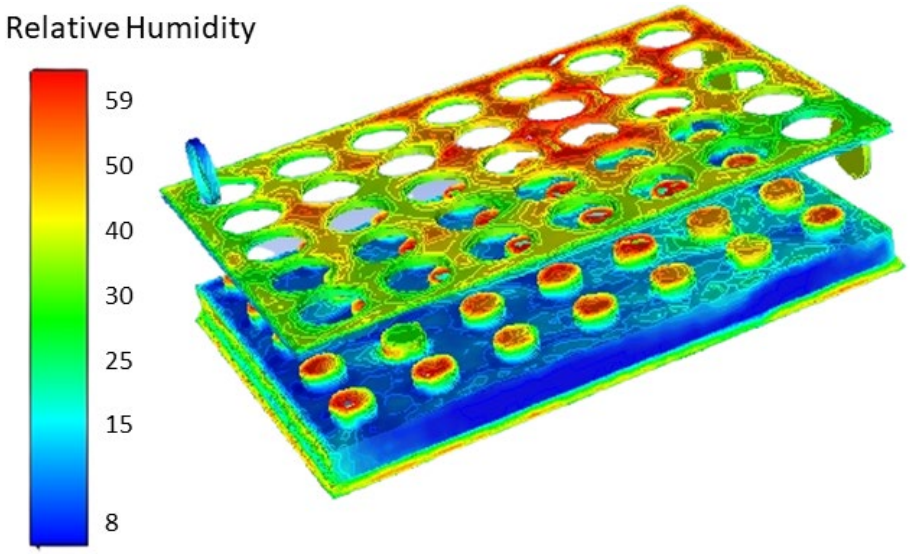


Figure 11. Spatial Distribution of Relative Humidity inside the Solar Greenhouse Dryer.

5. Validation

The comparative analysis presented in Table 8 validates the superiority of the proposed system compared to the existing systems. The modified greenhouse dryer under passive mode, implemented with the innovative modifications discussed in this study, demonstrates superior performance compared to the greenhouse under passive mode.

Table 8. Comparative table.

Sl. No.	System	U (W/m^2 K)	Characteristics Graph	Reference
1.	Modified greenhouse dryer under passive mode	3.78–4.46	Intercept at zero	[33]
2.	Greenhouse under passive mode	-	Intercept at zero	[34]
3.	Proposed System	3.87–5.03	Intercept at zero	

The proposed system showcases an improved range of overall heat transfer coefficients (U) compared to both the modified greenhouse dryer under passive mode and the conventional greenhouse under passive mode. This enhanced range (3.87–5.03 W/m^2 K) in the proposed system reflects its superior heat transfer capabilities and improved efficiency. Additionally, the characteristics graph of the proposed system intersects at zero, similar to the modified greenhouse dryer under the passive mode, indicating the validity and effectiveness of the modifications implemented in the proposed system. This comparative analysis further strengthens the conclusions drawn in this study, highlighting the superior performance of the proposed system compared to existing systems. The innovative modifications in the greenhouse dryer design contribute to its enhanced heat transfer efficiency and overall effectiveness in solar drying processes. These findings emphasize the significance and novelty of the proposed system in advancing the field of solar drying technologies.

6. Conclusions

The study presented herein focused on the design, fabrication, experimentation, and analysis of an innovative greenhouse dryer operating under natural convection mode in no-load conditions, with a particular emphasis on clear sky conditions. The primary objective was to enhance the classical even-span greenhouse dryer by incorporating hybrid thermal storage and a reflective mirror with thermocoal, thereby improving its drying efficiency. Through a comprehensive analysis of the experimental data and calculations of various heat transfer parameters, the following conclusions were drawn:

i. The variation of key parameters such as global solar radiation (GSR), ambient temperature, ambient relative humidity, and ambient wind speed followed regular patterns, with average values of 875.9 W/m^2, 31.98 °C, 40.08%, and 0.32 m/s, respectively.
ii. The indoor parameters of the proposed dryer, including inside temperature, inside relative humidity, ground temperature, and outlet temperature, exhibited regular variations, with average values of 41.25 °C, 35.31%, 61.65 °C, and 39.25 °C, respectively. The storage concept and reflective mirror contributed to elevated indoor temperatures, creating highly favorable conditions for drying and other thermal applications.
iii. Various mathematical parameters were evaluated to assess the thermal performance of the proposed system. The convective heat transfer coefficients from the ground and canopy, radiative heat transfer coefficient from the ground, and overall heat transfer coefficient showed hourly variations ranging from 2.47 to 3.55 W/m^2 K, 7.58 to 11.08 W/m^2 K, 6.05 to 7.39 W/m^2 K, and 3.87 to 5.03 W/m^2 K, respectively, with average values of 3.14 W/m^2 K, 8.43 W/m^2 K, 6.91 W/m^2 K, and 4.28 W/m^2 K, respectively.
iv. The characteristic graph for the proposed system, plotting the instantaneous thermal loss efficiency factor versus (Tr − Ta/Ir), intersected at zero, validating the modifications in the greenhouse dryer design. Heat loss varied from 105.58 to 549.42 W, with an average value of 428.33 W. The coefficient of diffusivity ranged from 0.1531×10^{-3} to 0.1547×10^{-3}, with an average value of 0.1541×10^{-3}.
v. Furthermore, dimensionless numbers including the Grashof number, Prandtl number, Rayleigh number, and Nusselt number were calculated. The Grashof number varied from 10×10^7 to 18×10^7, the Rayleigh number ranged from 2.69×10^7 to 5.85×10^7, and the Nusselt number showed variations from 27.63 to 38.39, with average values of 14×10^7, 4.1110×10^7, and 34.18, respectively. The Prandtl number remained almost constant at 0.69.
vi. The temperature distribution within the passive greenhouse dryer model ranged from 335 K to 310 K, providing an appropriate environment for natural convection-based product drying. The maximum relative humidity recorded in the greenhouse dryer was 59.8%, while the minimum relative humidity was 9.9%. Proper management of ventilation areas is crucial during periods of higher humidity to ensure optimal drying performance.
vii. Comparison with existing systems validated the superiority of the proposed system, exhibiting an improved range of overall heat transfer coefficients compared to the modified greenhouse dryer under passive mode and the conventional greenhouse under passive mode.

These findings highlight the enhanced heat transfer efficiency and overall effectiveness of the proposed innovative greenhouse dryer. The modifications implemented in the dryer design contribute to the advancement of solar drying technologies. The quantitative data and analysis presented in this study offer valuable insights for researchers, scientists, and entrepreneurs in the field of solar drying, paving the way for the development of sustainable and efficient drying systems.

7. Limitation of the Present Work

The present work is focused on no-load conditions under natural convection mode and clear sky conditions. While these conditions are important to evaluate the performance of the innovative greenhouse dryer, they may not fully capture its behavior under different operational scenarios and real-world conditions. Future studies should consider expanding the scope to include varying loads, weather conditions, and geographical locations to more comprehensively assess the dryer's performance. Also, the present study does not reflect the needs and requirements of large-scale applications. Investigating the system's performance with different crop types and varying drying capacities would provide a more comprehensive understanding of its versatility and applicability.

8. Future Scope

The study on the innovative greenhouse dryer presented in this work paves the way for future research and development in the field of solar drying. Several potential areas for further exploration arise from this study. First, future investigations can focus on evaluating the performance of the greenhouse dryer under extended operational conditions, including varying loads, diverse weather patterns, and different geographic locations. This will provide a more comprehensive understanding of its versatility and applicability. Second, researchers can explore the use of advanced materials, such as high-capacity phase change materials (PCMs), and innovative designs to further enhance the energy storage capabilities and overall efficiency of the system. Third, the integration of renewable energy sources, such as solar photovoltaic systems or wind turbines, presents an opportunity to augment the energy supply of the greenhouse dryer and reduce dependence on conventional energy sources. Fourth, the implementation of intelligent control systems and automation technologies can optimize the drying process by continuously monitoring and adjusting key parameters, resulting in improved efficiency, reduced energy consumption, and enhanced product quality. Finally, conducting comprehensive economic analyses and feasibility studies will be crucial to assess the cost-effectiveness and scalability of the proposed system, considering factors such as initial investment, operational costs, and potential savings. By addressing these areas of future research, solar drying technologies can be further advanced, leading to more sustainable, efficient, and economically viable drying solutions for various agricultural and industrial applications.

Author Contributions: Conceptualization, A.A., O.P., S.K.S., P.S.C., R.C. and S.S. methodology, A.A., O.P., S.K.S., P.S.C., R.C. and S.S.; formal analysis, A.A., O.P., S.K.S., P.S.C., R.C. and S.S.; investigation, A.A., O.P., S.K.S., P.S.C., R.C. and S.S.; writing—original draft preparation, A.A., O.P., S.K.S., P.S.C., R.C. and S.S.; writing—review and editing, S.S., R.K., S.M.T., A.K., B.S. and S.S.U.; supervision, S.S., R.K., S.M.T., A.K., B.S. and S.S.U.; project administration, S.S., B.S. and S.S.U.; funding acquisition, S.S., B.S. and S.S.U. All authors have read and agreed to the published version of the manuscript.

Funding: This study received funding from King Saud University, Saudi Arabia through researchers supporting project number (RSP2023R145). Additionally, the APCs were funded by King Saud University, Saudi Arabia through researchers supporting project number (RSP2023R145).

Institutional Review Board Statement: Not applicable.

Informed Consent Statement: Not applicable.

Data Availability Statement: No data were used to support this study.

Acknowledgments: The authors would like to thank King Saud University, Riyadh, Saudi Arabia, with researchers supporting project number RSP2023R145.

Conflicts of Interest: The authors declare no conflict of interest.

Nomenclature

Notation		Greek		Subscript	
A_{grd}	Ground area (m^2)	β_1	Coefficient of volumetric expansion (1/°C)	amb	ambient or air
B_1	Breadth of dryer (m)	γ	Relative humidity of air (%)	can	Canopy
C_p	Specific heat at constant pressure (J/kg °C)	ε	Emissivity	evp	Evaporative
C_{dif}	Coefficient of discharge	σ	Stefan–Boltzmann Constant ($W/m^2 K^4$)	grd	Ground
Gr	Grashof number	λ	Latent heat of vaporization (J/kg)	G	Ground to room
g	Acceleration due to gravity (m/s^2)	μ_1	Dynamic viscosity of air (kg/m)	I	Wall of greenhouse (0 to 5)
h	Heat transfer coefficients (W/m^2 °C)	ρ_1^+	Density of air (kg/m^3)	ra	Radiative
I	Solar intensity on greenhouse (W/m^2)	τ	Transmissivity	rm	Greenhouse air
K	Thermal conductivity (W/m °C)			vn	Vent
l	Thickness (m)			wd	Wind
Nu	Nusselt NumberParameter				
L_1	Length of the dryer (m)				
P(T)	vapor pressure at temperature T (N/m^2)				
P	Partial pressure difference between room temperature andambient air (N/m^2)				
Pr	Prandtl number				
Ra	Rayleigh number				
t	time in seconds				
T	Temperature (°C)				
U	Overall heat transfer coefficient (W/m^2 °C)				
V	Velocity (m/s)				
W_1	Characteristic dimension				

References

1. Chauhan, P.S.; Kumar, A.; Tekasakul, P. Applications of software in solar drying systems: A review. *Renew. Sustain. Energy Rev.* **2015**, *51*, 1326–1337. [CrossRef]
2. Ahmad, A.; Prakash, O.; Kumar, A.; Chatterjee, R.; Sharma, S.; Kumar, V.; Kulshreshtha, K.; Li, C.; Eldin, E.M.T. A Comprehensive State-of-the-Art Review on the Recent Developments in Greenhouse Drying. *Energies* **2022**, *15*, 9493. [CrossRef]
3. Chauhan, P.S.; Kumar, A. Performance analysis of greenhouse dryer by using insulated north-wall under natural convection mode. *Energy Rep.* **2016**, *2*, 107–116. [CrossRef]
4. Ahmad, A.; Prakash, O. Thermal analysis of north wall insulated greenhouse dryer at different bed conditions operating under natural convection mode. *Environ. Prog. Sustain. Energy* **2019**, *38*, e13257. [CrossRef]
5. Prakash, O.; Kumar, A. Solar greenhouse drying: A review. *Renew. Sustain. Energy Rev.* **2014**, *29*, 905–910. [CrossRef]
6. Ahmad, A.; Prakash, O.; Kumar, A.; Hussain, M.S. Drying kinetics and performance analysis of thermal storage-based hybrid greenhouse dryer for uniform drying of tomato flakes. *J. Therm. Sci. Eng. Appl.* **2023**, *15*, 050908. [CrossRef]
7. Chauhan, P.S.; Kumar, A. Heat transfer analysis of north wall insulated greenhouse dryer under natural convection mode. *Energy* **2016**, *118*, 1264–1274. [CrossRef]
8. Connellan, G.J. Greenhouse options for Southern Australian conditions. *Acta Hort* **1984**, *148*, 699–704. [CrossRef]
9. Sharma, A.; Kumar, D.; Kumar, A.; Faisal, N.; Kumar, N.; Pandey, S.; Hasnain, S.M.; Al-Hazani, T.M.; AlKahtane, A.A.; Alkahtani, S.; et al. Designing, Modeling, and Fabrication of a Novel Solar-Concentrating Spittoon against COVID-19 for Antibacterial Sustainable Atmosphere. *Sustainability* **2023**, *15*, 9286. [CrossRef]
10. Chauhan, P.S.; Kumar, A.; Gupta, B. A review on thermal models for greenhouse dryers. *Renew. Sustain. Energy Rev.* **2017**, *75*, 548–558. [CrossRef]
11. Zahid, M.S.; Ahmed, N.; Qaisrani, M.A.; Mahmood, M.; Ali, M.; Waqas, A.; Assadi, M. Charging and discharging characterization of a novel combined sensible-latent heat thermal energy storage system by experimental investigations for medium temperature applications. *J. Energy Storage* **2022**, *25*, 105612. [CrossRef]
12. Ahmad, A.; Prakash, O.; Kumar, A. Drying kinetics and economic analysis of bitter gourd flakes drying inside hybrid greenhouse dryer. *Environ. Sci. Pollut. Res.* **2021**, *30*, 72026–72040. [CrossRef] [PubMed]
13. Prakash, O.; Kumar, A. *Solar Drying Technology: Design, Testing, Modeling, Economics, and Environment*; Springer: Singapore, 2017; ISBN 978-981-10-3833-4.
14. Chauhan, P.S.; Kumar, A.; Nuntadusit, C.; Banout, J. Thermal modeling and drying kinetics of bitter gourd flakes drying in modified greenhouse dryer. *Renew. Energy* **2018**, *118*, 799–813. [CrossRef]

15. Chauhan, P.S.; Kumar, A.; Nuntadusit, C. Heat transfer analysis of PV integrated greenhouse dryer. *Renew. Energy* **2018**, *121*, 53–65. [CrossRef]
16. Berroug, F.; Lakhal, E.K.; El Omari, M.; Faraji, M.; El Qarnia, H. Thermal performance of a greenhouse with a phase change material north wall. *Energy Build.* **2011**, *43*, 3027–3035. [CrossRef]
17. Ayyappan, S.; Mayilsamy, K. Solar tunnel drier with thermal storage for drying of copra. *Int. J. Energy Technol. Policy* **2012**, *8*, 3–13. [CrossRef]
18. Ayyappan, S.; Mayilsamy, K.; Sreenarayanan, V.V. Performance improvement studies in a solar greenhouse drier using sensible heat storage materials. *Heat Mass Transf.* **2015**, *52*, 459–467. [CrossRef]
19. Ahmad, A.; Prakash, O. Performance evaluation of a solar greenhouse dryer at different bed conditions operating under passive mode. *J. Sol. Energy Eng. Incl. Wind. Energy Build. Energy Conserv.* **2020**, *142*, 011006.
20. Al-Obaidi, A.R.; Alhamid, J.; Khalaf, H.A. Effect of different corrugation interruptions Parameters on thermohydrodynamic characteristics and heat transfer performance of 3D Three-dimensional corrugated tube. *Case Stud. Therm. Eng.* **2022**, *32*, 101879. [CrossRef]
21. Tian, H.; Liu, J.; Wang, Z.; Xie, F.; Cao, Z. Characteristic Analysis and Circuit Implementation of a Novel Fractional-Order Memristor-Based Clamping Voltage Drift. *Fractal Fract.* **2023**, *7*, 2. [CrossRef]
22. Han, Y.; Chen, S.; Gong, C.; Zhao, X.; Zhang, F.; Li, Y. Accurate SM Disturbance Observer-Based Demagnetization Fault Diagnosis with Parameter Mismatch Impacts Eliminated for IPM Motors. *IEEE Trans. Power Electron.* **2023**, *38*, 5706–5710. [CrossRef]
23. Pan, X.; Wu, W.; Yu, X.; Lu, L.; Guo, C.; Zhao, Y. Typical electrical, mechanical, electromechanical characteristics of copper-encapsulated REBCO tapes after processing in temperature under 250 °C. *Supercond. Sci. Technol.* **2023**, *36*, 034004. [CrossRef]
24. Song, S.; Chong, D.; Zhao, Q.; Chen, W.; Yan, J. Numerical investigation of the condensation oscillation mechanism of submerged steam jet with high mass flux. *Chem. Eng. Sci.* **2023**, *270*, 118516. [CrossRef]
25. Liang, Y.; Li, J.; Xue, Y.; Tan, T.; Jiang, Z.; He, Y.; Pan, Y. Benzene decomposition by non-thermal plasma: A detailed mechanism study by synchrotron radiation photoionization mass spectrometry and theoretical calculations. *J. Hazard. Mater.* **2021**, *420*, 126584. [CrossRef]
26. Hu, W.; Wang, T.; Chu, F. A novel Ramanujan digital twin for motor periodic fault monitoring and detection. *IEEE Trans. Ind. Inform.* **2023**, 1–9. [CrossRef]
27. Wang, J.; Liang, F.; Zhou, H.; Yang, M.; Wang, Q. Analysis of Position, Pose and Force Decoupling Characteristics of a 4-UPS/1-RPS Parallel Grinding Robot. *Symmetry* **2022**, *14*, 825. [CrossRef]
28. Yin, L.; Wang, L.; Huang, W.; Liu, S.; Yang, B.; Zheng, W. Spatiotemporal Analysis of Haze in Beijing Based on the Multi-Convolution Model. *Atmosphere* **2021**, *12*, 1408. [CrossRef]
29. Yin, L.; Wang, L.; Zheng, W.; Ge, L.; Tian, J.; Liu, Y.; Yang, B.; Liu, S. Evaluation of Empirical Atmospheric Models Using Swarm-C Satellite Data. *Atmosphere* **2022**, *13*, 294. [CrossRef]
30. Yin, L.; Wang, L.; Huang, W.; Tian, J.; Liu, S.; Yang, B.; Zheng, W. Haze Grading Using the Convolutional Neural Networks. *Atmosphere* **2022**, *13*, 522. [CrossRef]
31. Rouissi, W.; Naili, N.; Jarray, M.; Hazami, M. CFD Numerical Investigation of a New Solar Flat Air-Collector Having Different Obstacles with Various Configurations and Arrangements. *Math. Probl. Eng.* **2021**, *2021*, 9991808. [CrossRef]
32. Mellalou, A.; Riad, W.; Hnawi, S.K.; Tchenka, A.; Bacaoui, A.; Outzourhit, A. Experimental and CFD Investigation of a Modified Uneven-Span Greenhouse Solar Dryer in No-Load Conditions under Natural Convection Mode. *Int. J. Photoenergy* **2021**, *2021*, 9918166. [CrossRef]
33. Prakash, O.; Anil Kumar, A. Annual Performance of Modified Greenhouse Dryer under Passive Mode in No-Load Conditions. *Int. J. Green Energy* **2015**, *12*, 1091–1099. [CrossRef]
34. Sutar, R.F.; Tiwari, G.N. Temperature reductions inside a greenhouse. *Energy* **1996**, *21*, 61–65. [CrossRef]

Disclaimer/Publisher's Note: The statements, opinions and data contained in all publications are solely those of the individual author(s) and contributor(s) and not of MDPI and/or the editor(s). MDPI and/or the editor(s) disclaim responsibility for any injury to people or property resulting from any ideas, methods, instructions or products referred to in the content.